

PHOTON-LIMITED DEBLURRING USING ALGORITHM UNROLLING

Yash Sanghvi, Abhiram Gnanasambandan, and Stanley H. Chan

School of Electrical and Computer Engineering, Purdue University
465 Northwestern Ave, West Lafayette, IN 47907

ABSTRACT

Image deblurring in a photon-limited condition is ubiquitous in a variety of low-light applications such as photography, microscopy and astronomy. However, the presence of photon shot noise due to a low-illumination and/or short exposure makes the deblurring task substantially more challenging than conventional deblurring. In this paper we present an algorithm unrolling approach that unrolls a Plug-and-Play algorithm using a fixed-iteration network. By changing the conventional two-variable splitting formulation of Plug-and-Play to an alternate three-variable splitting, we obtain a differentiable and end-to-end trainable network. Our algorithm outperforms existing methods for 1dB across different illuminations. We also overcome the difficulty of acquiring *real* motion blur kernels at low-light by presenting a photon-limited motion deblurring image dataset.

Index Terms— Poisson deconvolution, non-blind deblurring, photon-limited imaging, algorithm unrolling.

1. INTRODUCTION

Non-blind image deblurring is a restoration problem where the goal is to recover the clean image from an image corrupted by a spatially invariant blur due to motion, camera shake or defocus. This problem involves finding \mathbf{x} from the equation $\mathbf{y} = \mathbf{Hx} + \mathbf{n}$, where the \mathbf{x} is the clean image to be recovered, \mathbf{y} is the noisy blurry observation, \mathbf{H} is the blur represented in the matrix form, and \mathbf{n} is the additive i.i.d Gaussian noise. Non-blind deblurring methods assume that blur \mathbf{H} to be known.

An overwhelming majority of the existing deblurring solutions [1, 2, 3, 4, 5, 6] can handle the blur and the i.i.d Gaussian noise. However, in low-light settings, the images captured by the sensor are corrupted by Poisson shot noise. We refer to this situation as the *photon-limited* setting, i.e., when the average number of photons arriving at the image sensor during the exposure is small compared to that of a well-illuminated or *photon-abundant scene*. Note that photon noise is caused by the random nature of the photon arrivals that is present even if we have an ideal sensor. Existing deblurring algorithms fail to address the problem because of the strong noise.

1.1. Problem Formulation

We assume that the clean image $\mathbf{x} \in \mathbb{R}^N$ is normalized to $[0, 1]$ and is monochrome. It is blurred by a motion kernel \mathbf{H} . The signal-dependent shot noise is represented using the term *photon level* α and hence the sensor output is given by

$$\mathbf{y} = \text{Poisson}(\alpha \cdot \mathbf{Hx}), \quad (1)$$

where $\text{Poisson}(\mathbf{u})$ represents an instance of Poisson random vector with mean equal to \mathbf{u} . Therefore, the likelihood of the corrupted image \mathbf{y} given the clean signal \mathbf{x} is

$$p(\mathbf{y}|\mathbf{x}; \alpha) = \prod_{j=1}^N \frac{[\alpha \mathbf{Hx}]_j^{\mathbf{y}_j} e^{-[\alpha \mathbf{Hx}]_j}}{\mathbf{y}_j!}, \quad (2)$$

where $[\cdot]_j$ represents the j th entry of the vector. Framing the inverse problem as a maximum-a-posterior estimation, we aim to solve for \mathbf{x} from \mathbf{y} by maximizing the posterior probability.

1.2. Related work and contributions

The Poisson deconvolution problem has been studied for a long time [7, 8, 9] but their performance is limited because of the prior which is difficult to model for natural images. A possible solution is to incorporate a more powerful prior by means of deep neural networks. However, a brute-force end-to-end training of a generic network is sub-optimal because the forward model needs to be included. The two contributions of this paper are:

1. We propose a new method to unroll the Plug-and-Play algorithm [10, 11] using a fixed-iteration unrolled network [12]. Compared to prior work such as [13] which requires an inner iteration solver, our three-operator splitting strategy makes the sub-problems differentiable. See Figure 1 for our schematic diagram.
2. We overcome the difficulty of collecting low-light blurred images and the blur kernels. We demonstrate superior deblurring performance on *real* data as shown in Figure 2. We make this real dataset available.

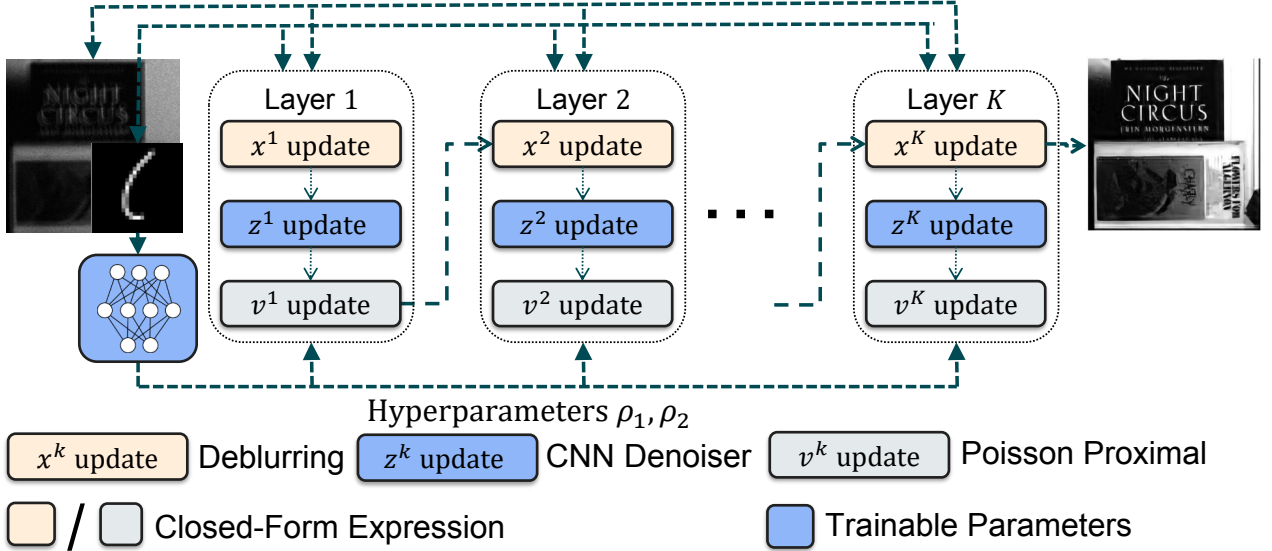


Fig. 1: Schematic diagram of results of the proposed method. We introduce an alternative formulation of the PnP problem so that each sub-module has a closed form so that it is differentiable.

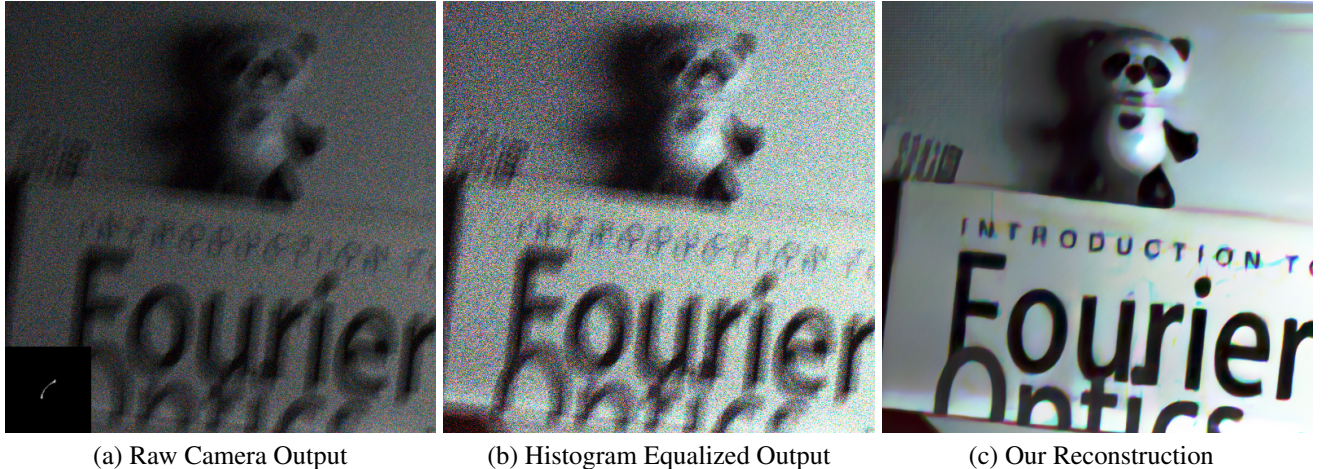


Fig. 2: Reconstruction of *real data* using the proposed method.

2. METHOD

The maximum-a-posteriori estimation is given by the minimization of the Poisson log-likelihood and the prior $p(\mathbf{x})$:

$$\mathbf{x}^* = \underset{\mathbf{x}}{\operatorname{argmin}} \left[\alpha \mathbf{1}^T \mathbf{H} \mathbf{x} - \mathbf{y}^T \log(\alpha \mathbf{H} \mathbf{x}) - \log p(\mathbf{x}) \right], \quad (3)$$

where $\mathbf{1}$ represents the all-one vector. The conventional approach to this problem is to adopt following the Plug-and-Play (PnP) framework [10, 11] with a two-variable splitting strategy:

$$\begin{aligned} \{\mathbf{x}^*, \mathbf{z}^*\} &= \underset{\mathbf{x}, \mathbf{z}}{\operatorname{argmin}} \left[-\mathbf{y}^T \log(\alpha \mathbf{H} \mathbf{x}) + \alpha \mathbf{1}^T \mathbf{H} \mathbf{x} - \log p(\mathbf{z}) \right] \\ \text{subject to } \mathbf{x} &= \mathbf{z}. \end{aligned} \quad (4)$$

Readers interested in the PnP derivation can consult work such as [10, 14]. What is worth noting is that the PnP algorithm

can be *unrolled* using a fixed iteration unrolling technique. However, while unrolling the PnP algorithm for a Gaussian likelihood has been demonstrated in many places, unrolling the PnP algorithm for a Poisson likelihood has never been reported. In particular, the subproblem involving the Poisson deblurring term does not pose a closed-form expression. Previous work such as [13] circumvents the issue by implementing an inner loop optimization. However, an inner loop solver in an unrolling network does not allow end-to-end training and is extremely inefficient.

The proposed method is inspired by the classical work of [15, 16]. In addition to splitting the variable as $\mathbf{x} = \mathbf{z}$, we introduce a third variable \mathbf{v} and write the optimization as

$$\begin{aligned} \{\mathbf{x}^*, \mathbf{z}^*, \mathbf{v}^*\} &= \underset{\mathbf{x}, \mathbf{z}, \mathbf{v}}{\operatorname{argmin}} \left[-\mathbf{y}^T \log(\alpha \mathbf{v}) + \alpha \mathbf{1}^T \mathbf{v} + \log p(\mathbf{z}) \right] \\ \text{subject to } \mathbf{x} &= \mathbf{z}, \quad \text{and} \quad \mathbf{H} \mathbf{x} = \mathbf{v}. \end{aligned} \quad (5)$$

The iterations of the algorithm are given by the following steps:

$$\mathbf{x}^{k+1} = (\mathbf{I} + (\rho_2/\rho_1)\mathbf{H}^T\mathbf{H})^{-1}(\tilde{\mathbf{x}}_0^k + (\rho_2/\rho_1)\mathbf{H}^T\tilde{\mathbf{x}}_1^k), \quad (6a)$$

$$\mathbf{z}^{k+1} = D_\sigma(\tilde{\mathbf{z}}^k), \quad (6b)$$

$$\mathbf{v}^{k+1} = \frac{-(\rho_2\tilde{\mathbf{v}}^k - \alpha) + \sqrt{(\rho_2\tilde{\mathbf{v}}^k - \alpha)^2 + 4\rho_2\mathbf{y}}}{2\rho_2}, \quad (6c)$$

$$\mathbf{u}_1^{k+1} = \mathbf{u}_1^k + \mathbf{x}^{k+1} - \mathbf{z}^{k+1}, \quad (6d)$$

$$\mathbf{u}_2^{k+1} = \mathbf{u}_2^k + \mathbf{H}\mathbf{x}^{k+1} - \mathbf{v}^{k+1}, \quad (6e)$$

where $\tilde{\mathbf{x}}_0^k \stackrel{\text{def}}{=} \mathbf{z}^{k+1} - \mathbf{u}_1^k$, $\tilde{\mathbf{x}}_1^k \stackrel{\text{def}}{=} \mathbf{v}^{k+1} - \mathbf{u}_2^k$, $\mathbf{v}^k \stackrel{\text{def}}{=} \mathbf{H}\mathbf{x}^k + \mathbf{u}_2^k$, $\tilde{\mathbf{z}}^k \stackrel{\text{def}}{=} \mathbf{x}^k + \mathbf{u}_1^k$, and D_σ denotes a denoiser with a hyperparameter σ .

The key observation here is that all the steps are in *closed-form* except for D_σ which is implemented as a neural network. Unrolling the resulting algorithm gives us the unrolled network shown in Figure 1. In our experiments, we unfolded the algorithm using $K = 8$ iterations. Since all the steps are *differentiable* in the sense of backpropagation, we can train the unrolled network end-to-end.

To train the above mentioned unrolled network, we use the multi-scale ℓ_1 loss such that the network output \mathbf{x}^K matches the clean image \mathbf{x} . To initialize \mathbf{x}^0 , we apply the classical Wiener filtering to obtain a rough estimate (do not confuse with [5]). The parameters used in updates (6a), (6c) - ρ_1^k, ρ_2^k for $k = 1, 2, 3, \dots, K$ are changed for each iteration and determined in one-shot by the blurring kernel \mathbf{h} and photon level α using a fully convolutional layer followed by a fully connected layer. For the denoiser in (6b), we use the architecture provided in [17] which introduces skip connections in a U-Net architecture known as ResUNet.

3. EXPERIMENTS

We evaluate our method using synthetically generated noisy blurred images on 100 images from the BSDS300 dataset [18]. We evaluate the performance on different photon levels ($\alpha = 5, 10, 20, 40$) representing various levels of degradation in terms of signal-to-noise ratio. We test the methods for different blur kernels - specifically 4 isotropic Gaussian kernels, 4 anisotropic Gaussian kernels, and 4 motion kernels. We also evaluated the methods on the dataset provided in Levin et. al [19]. This dataset contains a set of 32 blurred images generated by blurring 4 different clean images by 8 different motion kernels. We synthetically corrupt the blurred images with Poisson noise at different illumination levels.

We compare our method with the state-of-the-art Poisson deblurring algorithms: **RGDN** [1], **PURE-LET** [9], **DWDN** [5], and **DPIR** [20]. We retrained all the networks using the same Poisson data we used to train the proposed method. Hyperparameters are optimized to yield the best performance. The results for these evaluations are provided in Table 1 and Figure 3.

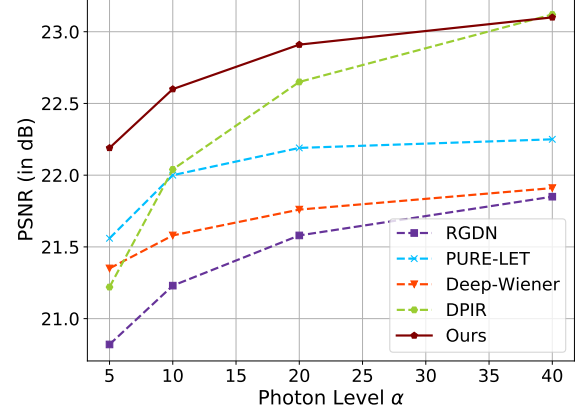


Fig. 3: PSNR values of synthetic experiments on the dataset in [19].

α	RGDN [1]	PURE-LET [9]	DWDN [5]	DPIR [20]	Ours
5	21.14	21.49	21.54	21.35	22.12
10	21.51	22.07	21.94	21.98	22.80
20	21.82	22.70	22.27	22.65	23.47
40	22.07	23.38	22.52	23.36	24.20

Table 1: PSNR values of synthetic experiments on BSD dataset for motion deblurring.

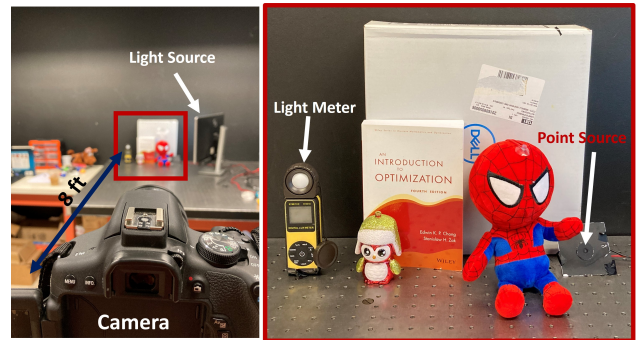


Fig. 4: Experimental Setup For evaluation of the proposed method on real images, we collect noisy and blurred images using a DSLR as shown in the setup shown above.

In addition to the above synthetic experiments, we built an optical experimental setup to collect the *real* motion blurred images as shown in Figure 4. We remark that this data collection is nontrivial because at low-light the blur kernel is much harder to obtain due to the shot noise. To overcome the difficulty, we first use an LCD monitor to project a uniform illumination to the scene. A light meter is installed to measure the lux level. To create a point source so that we track the motion trajectory (and hence the motion blur kernel), we placed a bright LED light behind a 30um pinhole cardboard. During the capture, we use a Canon T6i DSLR camera with f/5.0 and ISO 12800. The exposure time is controlled so that the average number of photons matches the α value. The captured blur

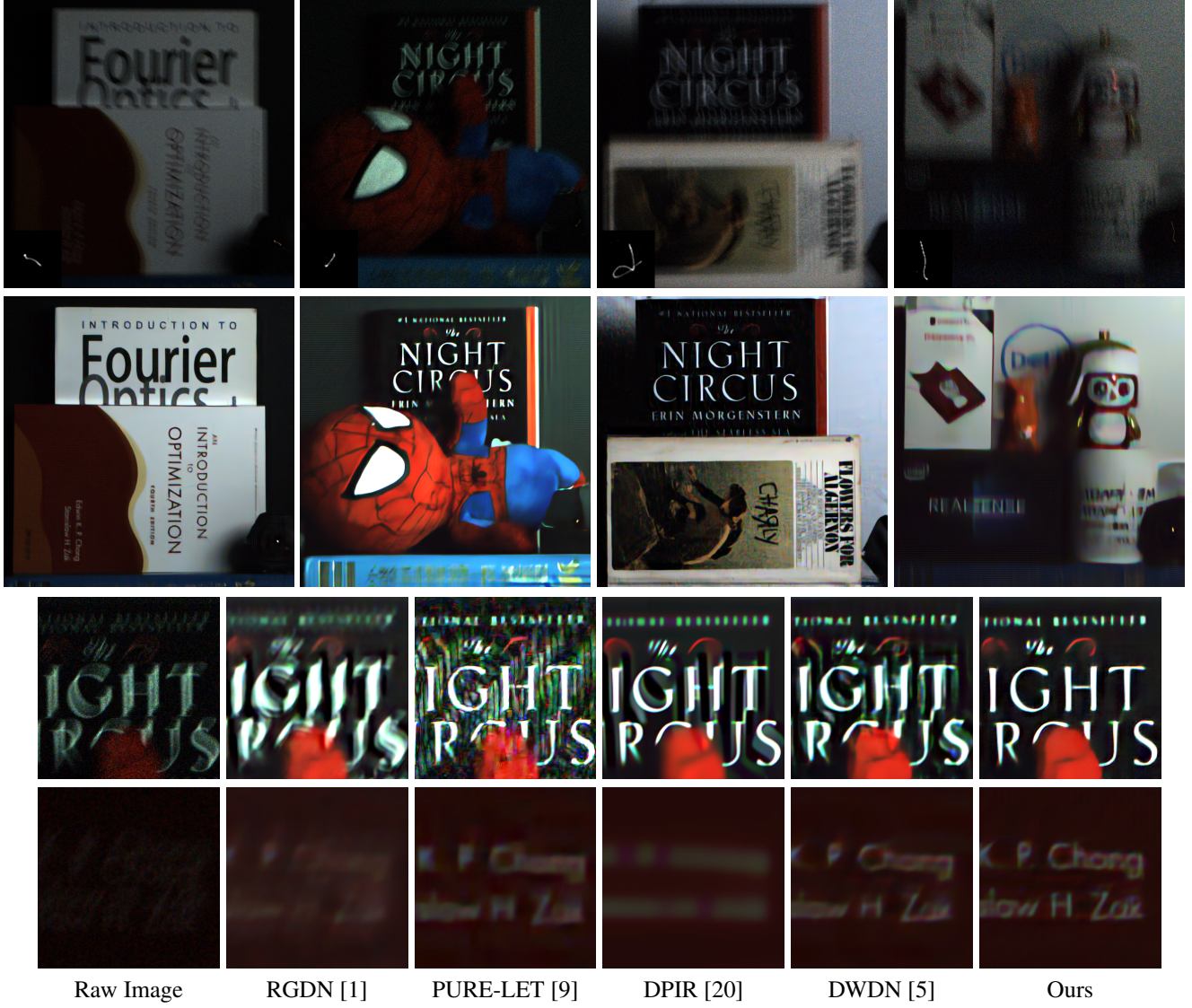


Fig. 5: [Top] Raw input and the proposed algorithm. [Bottom] Comparison with other methods.

kernels are denoised and post-processed before being used for evaluation. We have a total of 30 image and kernel pairs. The dataset will be released to the research community.

The qualitative experimental results are shown in Figure 5. It is evident from the results that the proposed method outperforms the competing methods by a big margin in terms of visual quality. In particular, we note that there are a substantial amount of ringing artifacts caused by RGDN [1], PURE-LET [9] and DWDN [5]. The results of DPIR [20] have fewer artifacts but the textures are oversmoothed. We also remark that RGDN, DWDN, and DPIR are deep learning algorithms that have been proven to outperform previous algorithms. Thus the superior performance of the proposed method over these methods means that it also outperforms other methods predicated. Due to space limit, the ablation studies are not included in this paper. However, we found that two-operator and three-operator

splitting approaches without unrolling performed much worse than the proposed three-operator splitting with unrolling, thus verifying the necessity of unrolling. The ablation results will be reported in a follow up journal paper.

4. CONCLUSION

Photon-limited deblurring has been an open problem for decades. Classical deterministic algorithms have limited performance due to the strong noise and weak priors. Deep learning algorithms have the capacity to learn a better prior but solving the Poisson posterior remains hard. We circumvent this bottleneck issue by proposing an unrolled three-operator splitting method. We demonstrated superior performance with a large margin compared to SOTA methods. We collected a real low-light dataset that will be released to the community.

5. REFERENCES

- [1] D. Gong, Z. Zhang, Q. Shi, A. van den Hengel, C. Shen, and Y. Zhang, “Learning deep gradient descent optimization for image deconvolution,” *IEEE Transactions on Neural Networks and Learning Systems*, vol. 31, no. 12, pp. 5468–5482, 2020.
- [2] Jakob Kruse, Carsten Rother, and Uwe Schmidt, “Learning to push the limits of efficient FFT-based image deconvolution,” in *Proceedings of the IEEE International Conference on Computer Vision*, 2017, pp. 4586–4594.
- [3] Thomas Eboli, Jian Sun, and Jean Ponce, “End-to-end interpretable learning of non-blind image deblurring,” in *Computer Vision–ECCV 2020: 16th European Conference, Glasgow, UK, August 23–28, 2020, Proceedings, Part XVII 16*. Springer, 2020, pp. 314–331.
- [4] Yuesong Nan, Yuhui Quan, and Hui Ji, “Variational-EM-based deep learning for noise-blind image deblurring,” in *Proceedings of the IEEE/CVF Conference on Computer Vision and Pattern Recognition*, 2020, pp. 3626–3635.
- [5] Jiangxin Dong, Stefan Roth, and Bernt Schiele, “Deep Wiener deconvolution: Wiener meets deep learning for image deblurring,” in *34th Conference on Neural Information Processing Systems*. Curran Associates, Inc., 2020.
- [6] Weisheng Dong, Peiyao Wang, Wotao Yin, Guangming Shi, Fangfang Wu, and Xiaotong Lu, “Denoising prior driven deep neural network for image restoration,” *IEEE transactions on pattern analysis and machine intelligence*, vol. 41, no. 10, pp. 2305–2318, 2018.
- [7] Zachary T Harmany, Roummel F Marcia, and Rebecca M Willett, “This is SPIRAL-TAP: Sparse Poisson intensity reconstruction algorithms—theory and practice,” *IEEE Transactions on Image Processing*, vol. 21, no. 3, pp. 1084–1096, 2011.
- [8] Robert D Nowak and Eric D Kolaczyk, “A statistical multiscale framework for Poisson inverse problems,” *IEEE Transactions on Information Theory*, vol. 46, no. 5, pp. 1811–1825, 2000.
- [9] Jizhou Li, Florian Luisier, and Thierry Blu, “Pure-let image deconvolution,” *IEEE Transactions on Image Processing*, vol. 27, no. 1, pp. 92–105, 2017.
- [10] Singanallur V Venkatakrishnan, Charles A Bouman, and Brendt Wohlberg, “Plug-and-play priors for model based reconstruction,” in *2013 IEEE Global Conference on Signal and Information Processing*. IEEE, 2013, pp. 945–948.
- [11] Stanley H Chan, Xiran Wang, and Omar A Elgendy, “Plug-and-play ADMM for image restoration: Fixed-point convergence and applications,” *IEEE Transactions on Computational Imaging*, vol. 3, no. 1, pp. 84–98, 2016.
- [12] Vishal Monga, Yuelong Li, and Yonina C Eldar, “Algorithm unrolling: Interpretable, efficient deep learning for signal and image processing,” *arXiv preprint arXiv:1912.10557*, 2019.
- [13] Arie Rond, Raja Giryes, and Michael Elad, “Poisson inverse problems by the plug-and-play scheme,” *Journal of Visual Communication and Image Representation*, vol. 41, pp. 96–108, 2016.
- [14] Suhas Sreehari, S Venkat Venkatakrishnan, Brendt Wohlberg, Gregory T Buzzard, Lawrence F Drummy, Jeffrey P Simmons, and Charles A Bouman, “Plug-and-play priors for bright field electron tomography and sparse interpolation,” *IEEE Transactions on Computational Imaging*, vol. 2, no. 4, pp. 408–423, 2016.
- [15] Mario AT Figueiredo and Jose M Bioucas-Dias, “Deconvolution of Poissonian images using variable splitting and augmented lagrangian optimization,” in *2009 IEEE/SP 15th Workshop on Statistical Signal Processing*. IEEE, 2009, pp. 733–736.
- [16] Mário AT Figueiredo and José M Bioucas-Dias, “Restoration of Poissonian images using alternating direction optimization,” *IEEE transactions on Image Processing*, vol. 19, no. 12, pp. 3133–3145, 2010.
- [17] Kai Zhang, Luc Van Gool, and Radu Timofte, “Deep unfolding network for image super-resolution,” in *Proceedings of the IEEE/CVF Conference on Computer Vision and Pattern Recognition*, 2020, pp. 3217–3226.
- [18] David Martin, Charless Fowlkes, Doron Tal, and Jitendra Malik, “A database of human segmented natural images and its application to evaluating segmentation algorithms and measuring ecological statistics,” in *Proceedings Eighth IEEE International Conference on Computer Vision. ICCV 2001*. IEEE, 2001, vol. 2, pp. 416–423.
- [19] Anat Levin, Yair Weiss, Fredo Durand, and William T Freeman, “Understanding and evaluating blind deconvolution algorithms,” in *2009 IEEE Conference on Computer Vision and Pattern Recognition*. IEEE, 2009, pp. 1964–1971.
- [20] Kai Zhang, Wangmeng Zuo, Shuhang Gu, and Lei Zhang, “Learning deep CNN denoiser prior for image restoration,” in *Proceedings of the IEEE Conference on Computer Vision and Pattern Recognition*, 2017, pp. 3929–3938.